Check for updates

JGR Space Physics

RESEARCH ARTICLE
10.1029/2026JA035864

Rapid Magnetotail Reconfiguration and Ion-Scale Wave Activity at Mercury

M. Persson[1], R. M. Dewey[2], A. I. Eriksson[1], M. André[1], E. Yordanova[1], L. Richard[1,3], A. Dagore[4,5], and J.-E. Wahlund[1]

[1]Swedish Institute of Space Physics, Uppsala, Sweden, [2]Climate and Space Sciences and Engineering, University of Michigan, Ann Arbor, MI, USA, [3]Rudolf Peierls Centre for Theoretical Physics, University of Oxford, Clarendon Laboratory, Oxford, UK, [4]Dipartimento di Fisica, Università di Trento, Povo, Italy, [5]Dipartimento di Fisica, Università della Calabria, Rende, Italy

Abstract Mercury's magnetosphere is an extremely dynamic environment, where substorm-like activity, including dipolarization fronts and particle acceleration, periodically disrupts the stability and radial extent of the closed field line region. The common narrowband ∼1 Hz waves at Mercury, near the local proton gyrofrequency are preferentially observed on closed field lines during quieter intervals, but their relationship to magnetospheric dynamics remains poorly understood. Here, we combine MESSENGER data sets of ∼1 Hz wave activity and dipolarization fronts to investigate whether newly closed field lines can sustain wave growth. We find that ∼1 Hz waves on the nightside are systematically absent during orbits with dipolarization intervals and typically confined within 1.3 R_M, compared to greater downtail extents during quiet intervals. The results indicate that ∼1 Hz waves require long-lived, stable closed field lines to grow; therefore, when they are observed, they can serve as diagnostics of Mercury's magnetospheric state, establishing a clear connection between field-line history, magnetospheric dynamics, and wave occurrence in Mercury's magnetotail.

Plain Language Summary Mercury has one of the most active and dynamic magnetic environments in the solar system. Like Earth, Mercury experiences bursts of magnetic activity called substorms, where energy stored in the magnetic tail is suddenly released, reshaping the magnetic field and accelerating particles. These reconfigurations produce sharp magnetic field signatures observable by spacecraft and dipolarization fronts, which can occur multiple times within minutes. Mercury's magnetosphere also hosts a common plasma wave oscillating at around 1 Hz, close to the frequency at which protons spiral around magnetic field lines. These waves are typically found in the quieter, more stable inner regions of the magnetosphere, but what controls their occurrence has been unclear. We combine two MESSENGER data sets, one cataloging ∼1 Hz waves and one cataloging dipolarization fronts, to investigate how magnetospheric activity affects wave occurrence. We find that the ∼1 Hz waves are systematically absent during orbits containing dipolarization fronts, and extend further down the magnetotail during quiet intervals. We interpret this as evidence that the waves require stable, long-lived magnetic field configurations to grow, conditions incompatible with the rapid field disruptions caused by dipolarization fronts. When detected, these waves can therefore serve as indicators of a relatively calm magnetospheric state.

Key Points:

- ∼1 Hz waves are systematically absent during orbits containing dipolarization intervals
- Newly closed field lines reconfigure on timescales of seconds, incompatible with the observed minutes of sustained ∼1 Hz wave activity
- Detected ∼1 Hz waves indicate the presence of stable closed field lines and a quiet magnetospheric state

Supporting Information:

Supporting Information may be found in the online version of this article.

Correspondence to:

M. Persson,
moa.persson@irf.se

Citation:

Persson, M., Dewey, R. M., Eriksson, A. I., André, M., Yordanova, E., Richard, L., et al. (2026). Rapid magnetotail reconfiguration and ion-scale wave activity at Mercury. *Journal of Geophysical Research: Space Physics*, *131*, e2026JA035864. https://doi.org/10.1029/2026JA035864

Received 29 JUN 2026
Accepted 13 SEP 2026

Author Contributions:

Conceptualization: M. Persson
Data curation: R. M. Dewey
Formal analysis: M. Persson
Funding acquisition: M. Persson, R. M. Dewey
Investigation: M. Persson, R. M. Dewey
Methodology: M. Persson, A. Dagore
Software: A. Dagore
Visualization: M. Persson
Writing – original draft: M. Persson
Writing – review & editing: M. Persson, R. M. Dewey, A. I. Eriksson, M. André, E. Yordanova, L. Richard, A. Dagore, J.-E. Wahlund

© 2026 The Author(s). Journal of Geophysical Research: Space Physics published by Wiley Periodicals LLC on behalf of American Geophysical Union. This is an open access article under the terms of the Creative Commons Attribution License, which permits use, distribution and reproduction in any medium, provided the original work is properly cited.

1. Introduction

Mercury has the smallest and most dynamic magnetosphere in the Solar System. The intrinsic dipole moment of Mercury is approximately two orders of magnitude weaker than that of Earth (Alexeev et al., 2010; Anderson et al., 2010, 2012), while the solar wind dynamic pressure at Mercury's orbit is substantially enhanced compared to that at Earth (W. Sun et al., 2022). The combination of a weak intrinsic magnetic field and enhanced upstream forcing results in a small and compressed magnetosphere, with a nominal subsolar standoff distance of 1.45–1.5 R_M (Winslow et al., 2013; Zhong, Wan, Slavin, et al., 2015). Under extreme conditions, such as strong dynamic pressures or extreme space weather events, the dayside magnetopause can even be compressed down to altitudes comparable to or below the planetary surface, effectively erasing the dayside magnetosphere (Jia et al., 2019; Slavin et al., 2019; Winslow et al., 2013, 2020; Zhong, Wan, Wei, et al., 2015).

The small spatial scale of the system implies a reduced separation between global and kinetic plasma scales. The ion inertial length and gyroradii for protons are both of order 100–200 km at typical magnetic fields of 60–100 nT, plasma densities of 1–5 cm^{-3} and energies of 1–3 keV (Gershman et al., 2014), while for heavier exospheric

21699402, 2026, 9, Downloaded from https://agupubs.onlinelibrary.wiley.com/doi/10.1029/2026JA035864 by Uppsala University Library, Wiley Online Library on [09/10/2026]. See the Terms and Conditions (https://onlinelibrary.wiley.com/terms-and-conditions) on Wiley Online Library for rules of use; OA articles are governed by the applicable Creative Commons License

species such as Na^+, these scales increase by up to an order of magnitude. These lengths thus represent a significant fraction of the magnetospheric dimensions, and ion kinetic processes therefore play a dominant role in governing magnetospheric dynamics. The Dungey cycle operates similarly at Mercury as at Earth, circulating magnetic flux and plasma through the system, but on much shorter time scales of 2–3 min at Mercury compared to several hours at Earth (Imber & Slavin, 2017; Slavin et al., 2010, 2021). During the unloading phase of the substorm, magnetic reconnection in the plasma sheet creates newly closed field lines convecting toward the planet (Slavin et al., 2009). The stretched magnetotail field lines will reconfigure toward a more dipolar configuration, which may be observed as a strong northward magnetic field component, called dipolarization fronts (DFs; Dewey et al., 2020; Sundberg et al., 2012). DFs at Mercury are frequent, observed in up to 50% of the MESSENGER orbits, but their occurrence is often asymmetric, with a preference of reconnection-related signatures of the plasma sheet toward the dawnside magnetotail (Boardsen et al., 2015; Dewey et al., 2020; Poh et al., 2017; W. J. Sun et al., 2017), a feature also observed at Earth but with an opposite asymmetry (e.g., Richard et al., 2022). However, during quiet intervals of the magnetosphere, substorm-type phenomena are typically absent, and drift physics dominates the magnetosphere (Korth et al., 2011; Slavin et al., 2018).

In parallel with reconnection-driven dynamics, Mercury's magnetosphere hosts a variety of plasma wave phenomena. Of particular interest are coherent narrowband waves observed near ∼1 Hz, close to the local proton gyrofrequency, first detected during the flybys of Mariner 10 (Russell, 1989) and later frequently observed by MESSENGER (Boardsen et al., 2009, 2012). These waves are typically found on closed field lines at L-shells <2 (Boardsen et al., 2012) and exhibit frequencies that decrease systematically relative to the proton cyclotron frequency at higher magnetic latitudes (Persson et al., 2026). In several cases, multiple harmonics above the fundamental mode have been reported (Boardsen et al., 2012, 2015). The wave mode responsible for these oscillations remains debated. Proposed interpretations include field line resonances, ion-ion hybrid waves, electromagnetic ion cyclotron (EMIC) waves, and electromagnetic ion Bernstein mode waves (Boardsen et al., 2015; Kim et al., 2011, 2013, 2015, 2016; Othmer et al., 1999). Ray-tracing simulations by Boardsen et al. (2015) demonstrated that the observed harmonic structure and frequency characteristics are broadly consistent with an "electromagnetic" variation of ion Bernstein mode waves under loss cone anisotropic particle distributions.

A full-mission statistical investigation by Persson et al. (2026) demonstrated that these ∼1 Hz waves occur preferentially on closed field lines under relatively quiet magnetospheric intervals, at up to 20% of the orbits passing through this region. The occurrence rate increases during northward interplanetary magnetic field (IMF) and decreases during southward IMF. Furthermore, the wave occurrence is inversely correlated with the Mercury Disturbance Index (MDI), a metric Anderson et al. (2013) derived from magnetic field fluctuations within the magnetosphere that ranks the disturbance level of all MESSENGER orbits. Together, these results indicate that the ∼1 Hz waves favor magnetospheric conditions characterized by reduced large-scale reconfigurations.

Since magnetospheric disturbance at Mercury is mostly governed by activity in the magnetotail, such as during substorms, with its unloading of the magnetotail and associated magnetic reconnection and DFs (Dewey et al., 2018; Imber & Slavin, 2017; W. J. Sun et al., 2017), the observed suppression of ∼1 Hz waves during disturbed intervals (Persson et al., 2026) suggests a possible physical connection between wave absence and the presence of newly closed magnetic field lines. The observations of DFs represent recently reconnected magnetic field lines that are undergoing rapid topological changes and are associated with strong plasma convection and heating (Dewey et al., 2017, 2018; W. J. Sun et al., 2017, 2018; Zhao et al., 2020; Zhong et al., 2018). Such conditions may inhibit the generation, growth, or maintenance of the wave mode responsible for the ∼1 Hz waves.

In this study, we investigate whether ∼1 Hz waves are absent on newly closed field lines in Mercury's magnetotail. By systematically comparing the intervals of dipolarization activity with the occurrence of coherent ∼1 Hz waves, we aim to quantify the relationship between reconnection-driven flux transport and wave occurrence. This analysis allows us to establish the temporal and physical conditions that may be necessary for wave activity, and to evaluate the ∼1 Hz waves as diagnostics of Mercury's magnetospheric disturbance state.

The following section describes the MESSENGER instrumentation and wave identification methodology, as well as the dipolarization event database used in this study. Section 3 presents the statistical results, Section 4 discusses their physical implications, and Section 5 summarizes the conclusions and provides predictions for future BepiColombo observations.

2. Instrumentation and Methods

In this study, we use the magnetometer (MAG; Anderson et al., 2007) data from the MESSENGER mission (Solomon et al., 2007). We use the full resolution 20 samples per second data from the full orbital period of the mission from March 2011 to April 2015, comprising over 4000 orbits in total. Additionally, we use proton energy spectra from the Fast Imaging Plasma Spectrometer (FIPS; Andrews et al., 2007) to provide context for the magnetospheric plasma conditions. FIPS measured the ion energy-per-charge (~0.05–20 keV/q) over an approximately 2π sr field-of-view, partially obstructed by spacecraft structures, limiting coverage of the full 3D velocity distribution. The MAG data were previously used to create a large data set of the presence of ~1 Hz waves in Mercury's magnetosphere (Persson et al., 2026), which we use here. The waves were identified through a semi-manual scheme that involved identifying coherent wave ridges typically near 0.5–2 Hz, which were required to be temporally and spectrally coherent for inclusion. A full description of the method and the wave identification is provided by Persson et al. (2026). The data set provides wave spectral properties as well as parallel and perpendicular wave power, which were used in this study to investigate their connection to dipolarization activity in the magnetotail.

In addition to the wave ridge event data set, we further characterize the wave activity using three complementary spectral methods. First, the wavelet method (Torrence & Compo, 1998) was used to determinate the wave ridge events, with an example shown in Figure 1. Second, the Fast Fourier Transform (FFT) method was used to investigate the presence or absence of wave activity during selected time intervals. Lastly, to investigate the potential presence of ~1 Hz wave activity during dipolarization events, where the general turbulent magnetic field activity was strong, the Empirical Mode Decomposition (EMD; Huang et al., 1998) method was used. Unlike the wavelet and FFT methods, EMD does not impose pre-defined criteria on the signal, making it a robust technique for processing nonlinear and nonstationary data. The method decomposes a signal into intrinsic mode functions ordered from higher to lower frequency components, which are then subjected to Hilbert spectral analysis to derive instantaneous amplitudes and frequencies in the time-frequency domain. EMD is finding increasing application in plasma physics to analyze turbulence and intermittency in solar wind and coronal mass ejections (Alberti et al., 2019; Carbone et al., 2018; Dagore et al., 2026). Further details on the method and its application are provided in Supporting Information S1.

Additionally, we include identified DFs within the plasma sheet of Mercury by Dewey et al. (2020). DFs were identified using an automated method: step-like increases in the northward component of the magnetic field (B_Z) are first detected using a sliding-window approach and then a series of physical tests are applied to determine which of these signals represent dipolarization events. This algorithm was optimized and then applied to 1946 magnetotail crossings that span the full orbital phase of the MESSENGER mission and cover the spatial region $-2.5 < X_{\mathrm{MSM'}} < 0\ R_M$, $|Y_{\mathrm{MSM'}}| < 1.5\ R_M$, and $|Z_{\mathrm{MSM'}}| < 0.2\ R_M$. A complete description of the methodology and spatiotemporal selection is provided by Dewey et al. (2020). Here, only the number of DFs present during each orbit is used. When combining the ~1 Hz wave data set with the DF data set from Dewey et al. (2020), the total number of orbits to use decreases from 2694 to 1120, still spanning the full mission over 2011 to 2015.

The results are analyzed in the Mercury Solar Orbital (MSO) coordinate system, in which X points from Mercury's geographical center toward the Sun, Z points along the angular momentum vector of the planet's motion around the Sun, and Y completes the right-handed orthogonal coordinate system. The Mercury Solar Magnetospheric (MSM) coordinate system is also used, which is identical to MSO but with its origin shifted from Mercury's geographical center to the center of the intrinsic magnetic dipole field at $Z_{\mathrm{MSO}} = 0.196\ R_M$ (Anderson et al., 2011). The DFs were identified in the MSM' coordinate system, which is identical to MSM but with the X-axis rotated about Z to align with the aberrated solar wind flow direction (assuming a radial solar wind speed of 400 km/s), accounting for Mercury's orbital motion. For the wave analysis, the Mean Field Aligned coordinate system is used, in which the parallel component is aligned with the local mean magnetic field direction (determined from a 100 s running mean), and the perpendicular components are defined in the plane normal to it (see Persson et al., 2026 for details). Additionally, the KT17 magnetic field model (Korth et al., 2017) is used to determine whether the spacecraft is expected to lie on an open or closed field line.

21699402, 2026, 9, Downloaded from https://agupubs.onlinelibrary.wiley.com/doi/10.1029/2026JA035864 by Uppsala University Library, Wiley Online Library on [09/10/2026]. See the Terms and Conditions (https://onlinelibrary.wiley.com/terms-and-conditions) on Wiley Online Library for rules of use; OA articles are governed by the applicable Creative Commons License

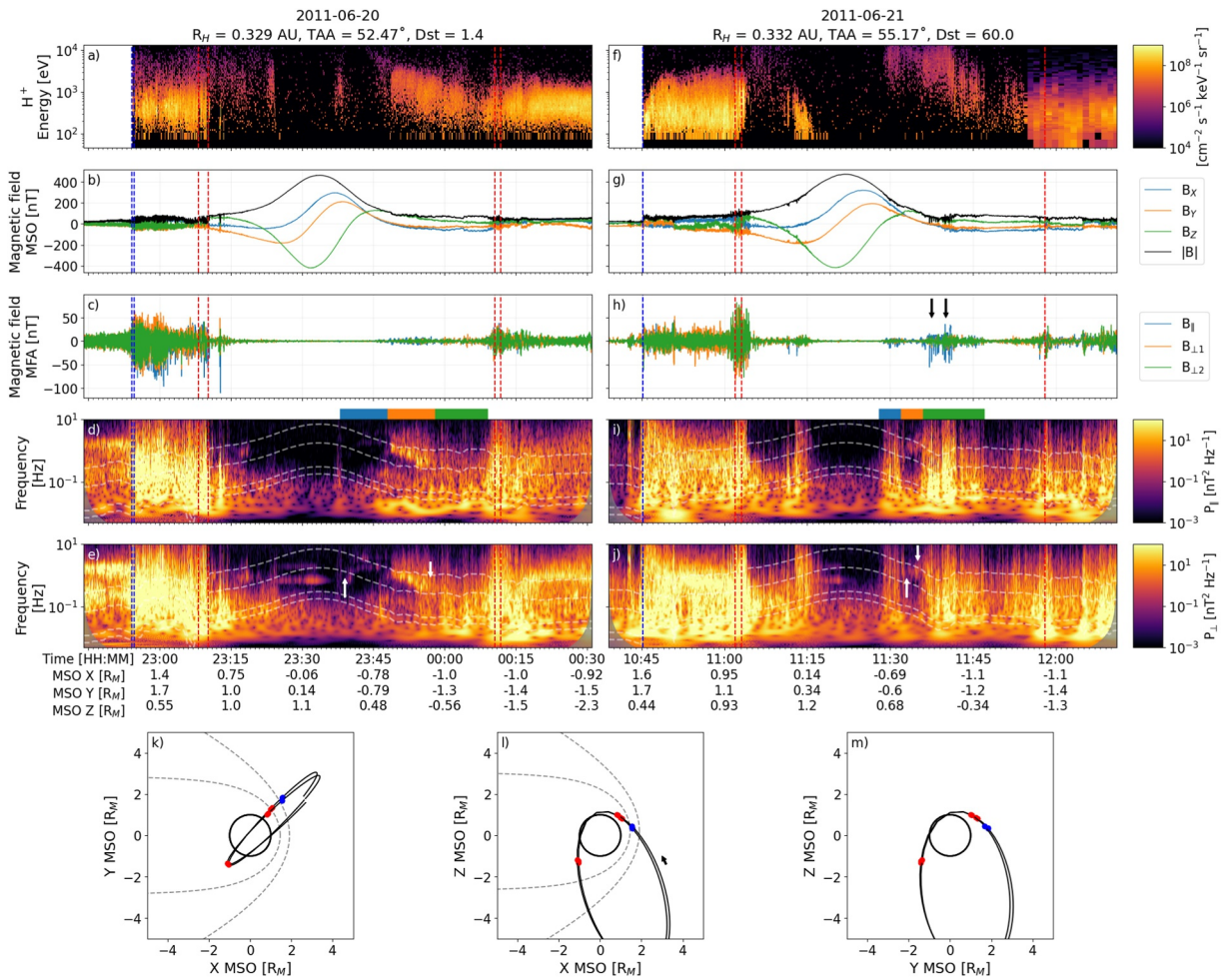

Figure 1. Two example orbits on 20 June 2011 (left) and 21 June 2011 (right). Panels show, from top to bottom: FIPS H^+ differential energy flux spectra (a, f), magnetic field components in Mercury Solar Orbital (b, g) and Mean Field Aligned coordinates (c, h); power spectral density as a function of frequency with parallel (d, i) and perpendicular components (e, j), and panels (k–m) the spacecraft trajectory in the magnetotail. White dashed lines mark the cyclotron frequencies of H^+, He^+, Na^+, and K^+ (top to bottom). The black arrow in panel (l) indicates the direction of spacecraft motion. Bow shock (blue) and magnetopause (red) crossings are marked in all panels, based on the crossing times identified by W. Sun (2023), with average locations from Winslow et al. (2013). Colored bars above panels (d) and (i) indicate the time intervals used for the Fast Fourier Transform analysis shown in Figure 2 and for the EMD analysis in Supporting Information S1. The black arrows in panel (h) indicate the first and last identified DFs from Dewey et al. (2020), while the white arrows in panels (e) and (j) indicate the start and end of the identified ~1 Hz wave intervals.

3. Results

3.1. The Orbits of 20 and 21 June 2011

To illustrate the effect of magnetospheric dynamics on the ~1 Hz waves, we compare two consecutive orbits from 20 to 21 June 2011 (Figure 1), whose pericenters are separated by ~12 hr and follow nearly identical trajectories (Figures 1i and 1j). The first orbit on 20 June is relatively undisturbed, with no identified DFs during the magnetotail crossing and stable closed field line configurations with associated high-energy semi-trapped ring current ions near ~23:45 (Zhao et al., 2022). In contrast, the second orbit on 21 June contains six identified DFs between ~11:30 and 11:45 (between the two black arrows in panel h, from Dewey et al., 2020), with associated highly accelerated protons, indicating active magnetotail reconfiguration (W. J. Sun et al., 2017). Following the nomenclature of Glass et al. (2022), the second orbit likely passed through the plasma sheet horns, with accelerated ions and broadband wave emissions, before briefly entering the closed field line region at ~11:35, where the proton energy distribution resembles that of the first orbit. The spacecraft subsequently crossed the central plasma sheet, where at least six DFs were identified using the automated procedure of Dewey et al. (2020) (black arrows, Figure 1h), alongside observations of accelerated protons. Correspondingly, the first orbit exhibits ~1 Hz

21699402, 2026, 9, Downloaded from https://agupubs.onlinelibrary.wiley.com/doi/10.1029/2026JA035864 by Uppsala University Library, Wiley Online Library on [09/10/2026]. See the Terms and Conditions (https://onlinelibrary.wiley.com/terms-and-conditions) on Wiley Online Library for rules of use; OA articles are governed by the applicable Creative Commons License

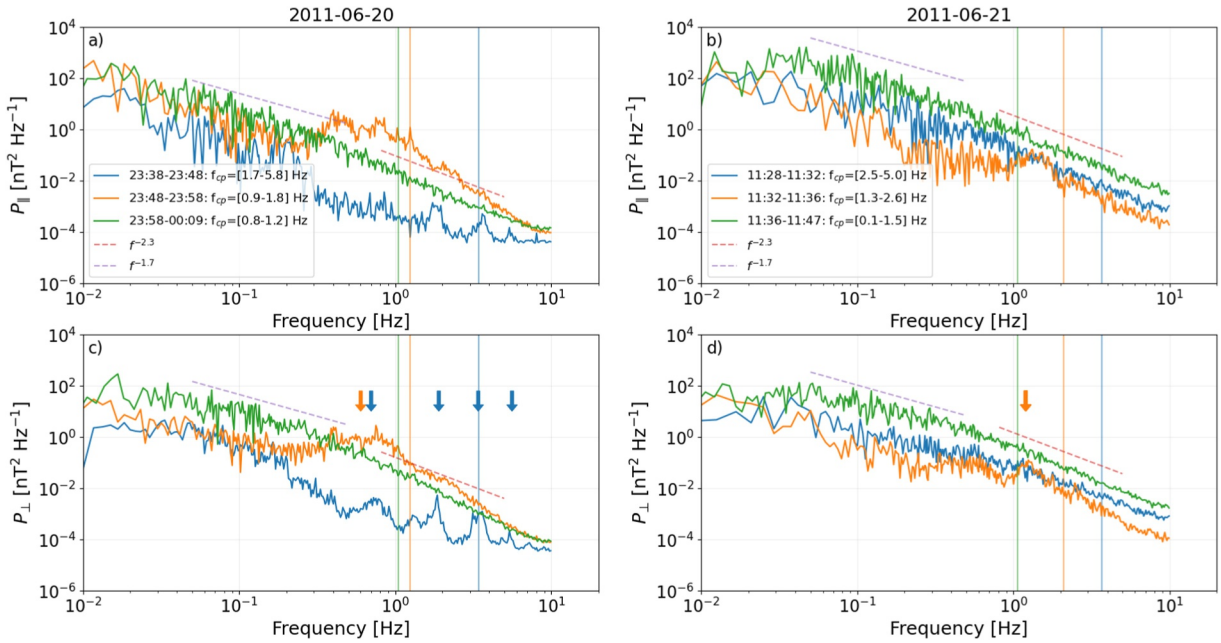

Figure 2. Power spectral density (PSD) comparisons for three selected intervals in each of the two orbits are shown in Figure 1. Panels (a) and (c) correspond to the 20 June orbit, and panels (b) and (d) to the 21 June orbit. Panels (a and b) show the parallel component PSD, while panels (c and d) show the perpendicular component. The analyzed intervals are indicated by the colored horizontal bars in Figure 1. Dashed lines indicate typical spectral indices reported for Mercury's magnetotail (Li et al., 2026). Arrows mark the ∼1 Hz peaks observed during the respective intervals. The colored vertical lines indicate the mean local proton cyclotron frequency (f_{cp}) for each time interval, with the range shown in the legend indicating the minimum and maximum f_{cp} values over that interval.

wave activity from 23:40 to 00:00 (marked by white arrows in panel e), with weak but coherent wave signatures from ∼23:40 to 23:47 (blue bar above panel 1d) that become significantly stronger after ∼23:47 (orange bar). The second orbit shows nearly no sustained narrowband wave activity near ∼1 Hz. The exception is a small region of small-amplitude, narrowband (∼1 Hz) wave activity near ∼11:35 (white arrows in panel j), appearing between broadband intervals, consistent with the brief closed-field-line interval identified at that time. The white dashed lines in panels 1d, 1e and 1i, 1j indicate the local gyrofrequencies of H^+, He^+, Na^+, and K^+ (top to bottom). The ∼1 Hz waves are typically close to, or slightly below, the local proton gyrofrequency, with a characteristic decrease relative to the proton gyrofrequency at locations above the magnetic equator ($Z_{MSO} > 0.196\ R_M$).

Figure 2 shows comparisons of power spectral density (PSD) from FFT for three selected intervals in each of the two example orbits, indicated by the colored bars in Figure 1. The intervals were selected based on their wavelet characteristics.

For the 20 June orbit, the first two intervals exhibit clear ∼1 Hz wave signatures, in agreement with the wavelet analysis in Figure 1. The first interval (blue) shows relatively low overall power but distinct narrowband peaks just below ∼1 Hz together with several harmonic peaks at higher frequencies. The second interval displays higher PSD levels and a broader ∼1 Hz peak. The increased peak width is partly due to the longer time window, during which the wave frequency varies (Figures 1d and 1e). For both intervals, the peaks are close to but below the local proton gyrofrequency (vertical lines), with the first interval's peak sitting notably further below. These variations in frequency and power are consistent with previously reported latitudinal dependence as the spacecraft moves from higher to lower magnetic latitudes (Persson et al., 2026).

The third interval of the 20 June orbit (green) shows a broadband spectrum without distinct ∼1 Hz peaks. Although a dedicated turbulence analysis is out of scope for this study, the spectral slopes are broadly consistent with the findings of Li et al. (2026) near Mercury's magnetotail current sheet, and of Richard et al. (2024) near Earth's magnetotail plasma sheet. Consistent with their findings, we find that the lower-frequency part shows a spectral slope that approximately follows the Kolmogorov index (−5/3), and the higher-frequency range shows a slope that is slightly harder than the typical −2.3 reported by Li et al. (2026) near the current sheet crossings.

21699402, 2026, 9, Downloaded from https://agupubs.onlinelibrary.wiley.com/doi/10.1029/2026JA035864 by Uppsala University Library, Wiley Online Library on [09/10/2026]. See the Terms and Conditions (https://onlinelibrary.wiley.com/terms-and-conditions) on Wiley Online Library for rules of use; OA articles are governed by the applicable Creative Commons License

21699402, 2026, 9, Downloaded from https://agupubs.onlinelibrary.wiley.com/doi/10.1029/2026JA035864 by Uppsala University Library, Wiley Online Library on [09/10/2026]. See the Terms and Conditions (https://onlinelibrary.wiley.com/terms-and-conditions) on Wiley Online Library for rules of use; OA articles are governed by the applicable Creative Commons License

In contrast, the 21 June orbit shows predominantly broadband spectra in all three intervals. The first (blue) and third (green) intervals, where the latter is the interval with the identified DFs, exhibit spectral slopes consistent with typical indices found at Mercury (Li et al., 2026). Similarly to what was found in Figure 1, the middle interval (orange) contains weak, broad enhancements near ∼1 Hz, although the degree of polarization (not shown) is lower than typically observed for the ∼1 Hz wave ridges, indicating a less organized wave field. Both wavelet and FFT analyses therefore confirm the absence of sustained narrowband ∼1 Hz waves during intervals with DFs. The wavelet and FFT methods use different assumptions in their frequency analysis, and their similar results indicate that the suppression is not due to temporal smoothing or spectral leakage. Furthermore, the estimated background noise of the MESSENGER fluxgate magnetometer is well below the amplitude of typical ∼1 Hz waves, confirming that the suppression is physical rather than a detection limitation.

To better exclude the possibility that the waves are masked by large-scale fluctuations, such as the strong MSO B_Z component of the DFs, we applied the EMD method to decompose the magnetic field data into intrinsic mode functions that correspond to different oscillatory components of the magnetic field signal. The results are included in Supporting Information S1, where the decomposition of the magnetic field signal into intrinsic mode functions for the two orbits is shown in Figures S1 and S2 in Supporting Information S1, respectively, and the resulting marginal Hilbert spectrum for each intrinsic mode function is included in Figure S3 in Supporting Information S1. The results from EMD provide the same conclusion as the FFT spectra, with no peaks appearing for the times of the identified DFs in the green interval in Figure 1. Unlike Fourier-based methods, EMD makes no prior assumptions about the stationarity or periodicity of the input signal but instead extracts the intrinsic mode functions adaptively. This ensures that the resulting Hilbert spectrum is not affected by large-scale fluctuations in the input signal, such as those associated with DFs. Thus, the EMD method strongly supports the conclusion that ∼1 Hz wave activity is suppressed, or absent, during intervals when the spacecraft is located on field lines associated with DFs.

3.2. Statistical Distributions of Waves Depending on Presence of Dipolarizations

The direct orbit-to-orbit comparison in the previous section exemplified that the absence of ∼1 Hz waves in the observations is associated with dynamical reconfiguration of the magnetic field, and not solely spatial location. To investigate if this broadly applies to the Mercury system, we can calculate the statistical relation between dipolarizations and ∼1 Hz waves in Mercury's magnetotail by combining the dipolarization event data set from Dewey et al. (2020) with the wave observation data set from Persson et al. (2026). The results are shown in the MSM X-Y plane in Figure 3, where the left column shows the occurrence rate of the ∼1 Hz waves on orbits where no DFs were detected during plasma sheet crossings, while the middle column includes orbits with at least one identified DF.

Orbits with zero DFs exhibit strong ∼1 Hz wave activity across the nightside and the region of wave activity extends to large radial distances from the planet. On the other hand, orbits containing DFs show almost a complete suppression of these waves at large distances, with a presence only very close to the planet. Also shown in panels (a1 and a2) is the proton plasma beta = 1 contour in the nightside, calculated from FIPS measurements by Dewey et al. (2020). Planetward of this boundary, the magnetic pressure dominates over the plasma pressure ($\beta < 1$), while tailward the plasma pressure dominates ($\beta > 1$). The ∼1 Hz wave occurrence broadly follows this contour in both groups, consistent with the waves being confined to the magnetically dominated closed field line region. The second row of Figure 3 shows the total number of magnetic field vector measurements for each group, where besides the terminator region, there is a uniform spatial coverage for both, which confirms that the absence of ∼1 Hz waves is not due to limitations in spatial coverage. The rightmost column of Figure 3 is an integration of all wave events for the local times 21:00–03:00 (indicated by the white dashed lines in panels (a1 and a2)). The data here are simply plotted against the radial distance from the magnetic field dipole center of the planet (MSM origin). The results further demonstrate that the radial extent of the wave region for the orbits where DFs were observed is very limited, almost entirely confined to regions near the planet, and occurs at a much lower rate than in the case where no DFs were identified.

We quantified the stability of ∼1 Hz waves by estimating the duration of their ridge-like signatures observed along the MESSENGER trajectory for each orbit using the full wave data set from Persson et al. (2026). Due to MESSENGER's elliptical orbit with a pericenter near the north pole, the spacecraft typically crossed the closed field line region twice per orbit, allowing the detection of up to two observable wave ridges per orbit. Figure 4 shows the distribution of the wave ridge duration for all events (blue), orbits with zero identified DFs (orange), and orbits with ≥1 identified DFs (green), separated into nightside and dayside intervals, with a comparison to the

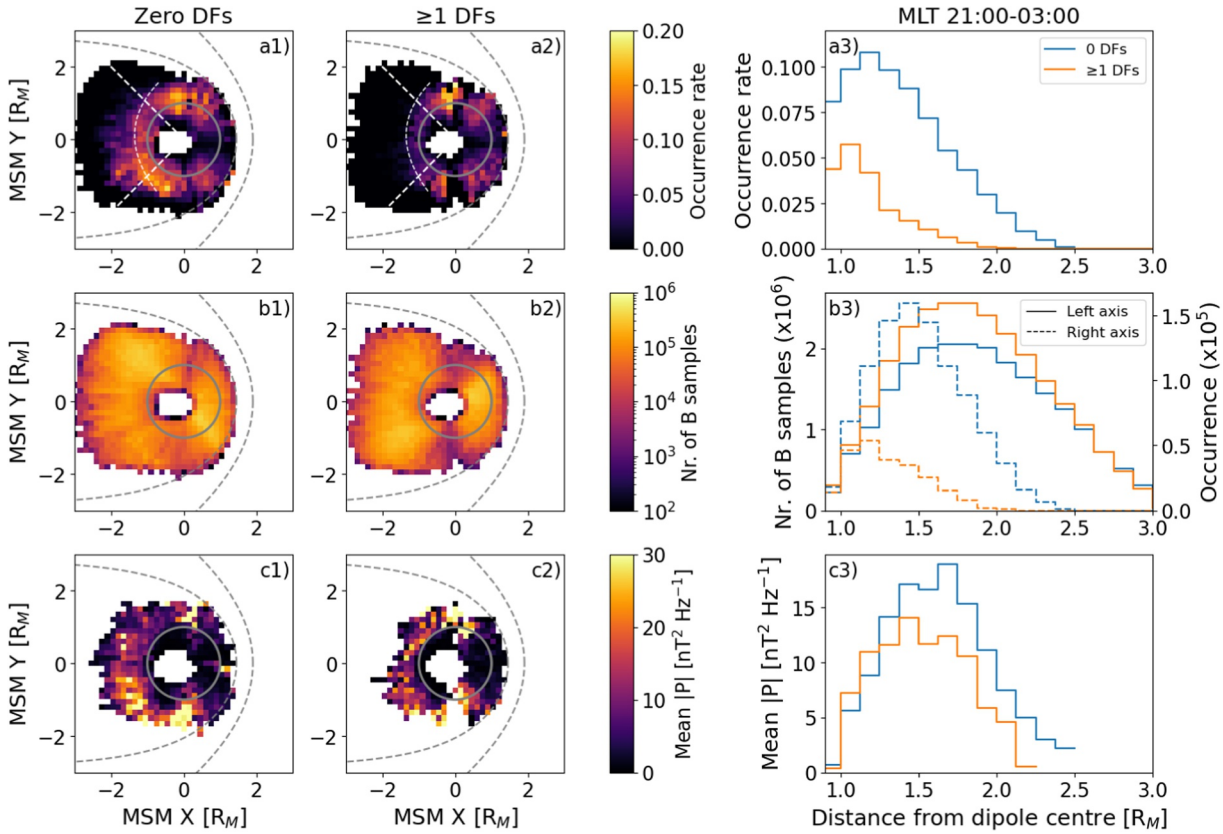

Figure 3. Observations of ∼1 Hz waves during orbits when zero (left column: a1, b1, c1) and ≥1 (middle column: a2, b2, c2) DFs were identified in the magnetotail plasma sheet crossings. The rightmost column (a3, b3, c3) shows an integrated histogram of the radial distribution from the magnetic dipole center of wave events for local times 21:00–03:00 (white dashed lines in left panels), with zero DFs in blue and ≥1 DFs in orange. Each row shows: (a1–a3) wave occurrence rate, (b1–b3) total number of magnetic field vector measurements (right axis in panel (b3) shows total wave occurrence), and (c1–c3) average ∼1 Hz wave power. The average bow shock and magnetopause (Winslow et al., 2013) are shown as dashed grey lines, and Mercury's outline as a solid grey line. The white dashed curve in panels (a1 and a2) shows the proton plasma beta = 1 contour in the magnetic equatorial plane ($Z_{MSM} \approx 0$) from the polynomial fit of Dewey et al. (2020), based on MESSENGER FIPS data.

total time spent on closed field lines. Wave ridges persist for ∼15 min on average, ranging from a few minutes up to ∼30 min. Dayside ridges are shorter (∼10 min) and show no dependence on DF occurrence, which is expected given that the identified DFs are confined to the nightside magnetotail. On the nightside, orbits containing DFs exhibit shorter ridge durations (<20 min, averaging ∼10 min) compared to up to 30 min (average ∼15 min) for orbits without identified DFs. This result further strengthens the conclusion that rapid magnetic reconfigurations, such as DFs, disrupt wave stability. These results complement Figure 3, showing that within DFs-rich orbits, nightside ∼1 Hz waves are confined to tightly bound closed field lines, whereas in DFs-free orbits, waves persist over larger spatial extents, and can therefore be observed for a longer time period along MESSENGER's trajectory. Overall, these observations underscore the critical role of the magnetospheric configuration in sustaining ∼1 Hz wave activity at Mercury.

4. Discussion

The case study (Figures 1 and 2) and the statistical analysis (Figures 3 and 4) together suggest that DFs and ∼1 Hz waves are generally mutually exclusive phenomena in the magnetotail of Mercury. During dynamic intervals, wave activity is spatially confined to the innermost closed field lines, in stark contrast to the large radial extent observed during quiet intervals (Figure 3). These results are consistent with the absence of ∼1 Hz waves on newly closed and dynamically reconfigured field lines. This indicates that rapid magnetotail reconfiguration does not provide the necessary conditions required for wave growth.

Under stable closed field line conditions, protons undergo repeated bounce motion over many gyroperiods, allowing pitch angle anisotropies consistent with loss cone distributions to develop (Zhao et al., 2022). Boardsen

21699402, 2026, 9, Downloaded from https://agupubs.onlinelibrary.wiley.com/doi/10.1029/2026JA035864 by Uppsala University Library, Wiley Online Library on [09/10/2026]. See the Terms and Conditions (https://onlinelibrary.wiley.com/terms-and-conditions) on Wiley Online Library for rules of use; OA articles are governed by the applicable Creative Commons License

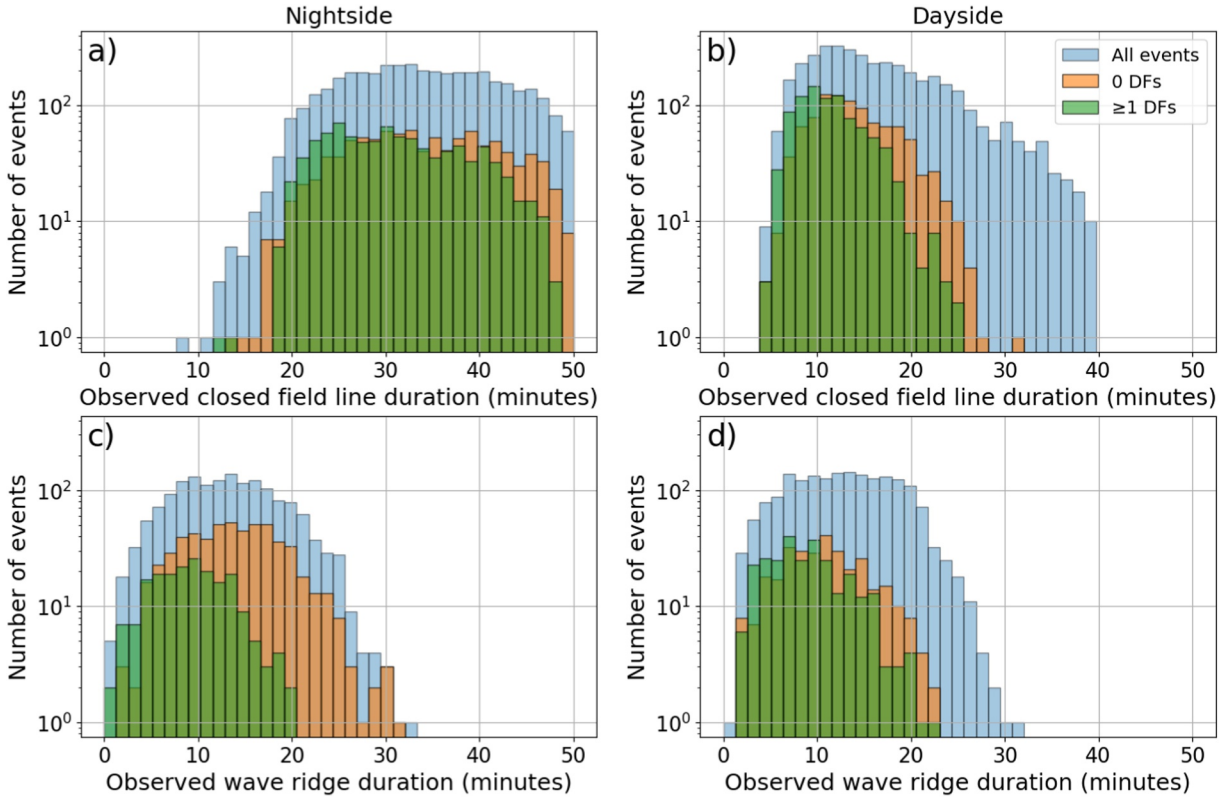

Figure 4. Distribution of observed ∼1 Hz wave ridge durations along MESSENGER trajectories. Data are grouped by all wave events (blue), orbits with zero DFs (orange), and orbits with ≥1 DFs (green). Panels show time spent on closed field lines per orbit, as identified from KT17 field line tracing, for (a) nightside and (b) dayside, and duration of wave ridges for (c) nightside and (d) dayside. DF statistics are used for orbits where ∼1 Hz wave events were identified; "all events" include all orbits with observed ∼1 Hz waves.

et al. (2015) showed that such loss cone distributions can drive ion Bernstein-mode or EMIC mode waves at Mercury, which are generally proposed to explain the observed ∼1 Hz waves (Boardsen et al., 2015; Cushen et al., 2025; Kim et al., 2016). Previous polarization analyses by Boardsen et al. (2012) found that the waves show a latitude-dependent polarization character, being more compressional with higher ellipticity near the magnetic equator and transitioning to transverse waves at higher latitudes, with wave normal angles peaked near 90°. These properties are consistent with quasi-perpendicular propagation and the electromagnetic ion Bernstein mode interpretation of Boardsen et al. (2015). The statistical properties of the ∼1 Hz waves in the database from Persson et al. (2026) are fully consistent with these findings. Full mode identification is beyond the scope of this study as it is not possible with the available instrumentation on MESSENGER. Future BepiColombo/Mio observations with electric and magnetic field measurements together with full pitch angle distributions (PADs) of ions and electrons should be able to provide a definitive mode evaluation of the ∼1 Hz waves and are therefore left as a future exercise for that mission. A larger discussion of the hypothesized wave modes, generation regions, and prospects for BepiColombo to definitively test these interpretations is provided by Persson et al. (2026).

The lack of ∼1 Hz wave activity during DF intervals can be understood in this context by comparing the characteristic time scales of the system. DFs at Mercury occur on time scales of 2–20 s (Dewey et al., 2020; Zhong et al., 2018), and can occur multiple times within a few minutes, continuously changing the magnetic field configuration (Sundberg et al., 2012; Zhong et al., 2019). The typical bounce period of a proton on a field line that crosses the equator at 1.3 R_M is 10–20 s (assuming a typical proton energy of a few keV and a magnetic field magnitude of ∼50–100 nT; Dewey et al., 2020). Since the DF timescales are shorter than or comparable to the proton bounce period, the magnetic field configuration on newly closed field lines may never remain stable long enough for a loss cone to establish itself. Even if a loss cone briefly forms, sustaining the anisotropic distribution required for ∼1 Hz wave growth seems to demand that the field remains stable for longer than the DF recurrence timescale, conditions that are fundamentally incompatible with the rapid and repeated field reconfiguration

21699402, 2026, 9, Downloaded from https://agupubs.onlinelibrary.wiley.com/doi/10.1029/2026JA035864 by Uppsala University Library, Wiley Online Library on [09/10/2026]. See the Terms and Conditions (https://onlinelibrary.wiley.com/terms-and-conditions) on Wiley Online Library for rules of use; OA articles are governed by the applicable Creative Commons License

21699402, 2026, 9, Downloaded from https://agupubs.onlinelibrary.wiley.com/doi/10.1029/2026JA035864 by Uppsala University Library, Wiley Online Library on [09/10/2026]. See the Terms and Conditions (https://onlinelibrary.wiley.com/terms-and-conditions) on Wiley Online Library for rules of use; OA articles are governed by the applicable Creative Commons License

associated with DFs at Mercury. This is consistent with observations of proton energization during DF intervals, which show perpendicular temperature anisotropy through betatron acceleration but without the organized loss cone structure in the PAD (Dewey et al., 2017; W. J. Sun et al., 2017) that is specifically proposed to provide the free energy for ∼1 Hz wave growth (Boardsen et al., 2015). These time scales are also significantly shorter than the duration of the observed ∼1 Hz waves, which can persist up to 20–30 min along the spacecraft trajectory, albeit with observed ridge-internal power variations.

Observations of DFs indicate the presence of newly closed field lines, which are convecting toward the planet. These field lines map to the planetary surface slightly equator-ward of the open-closed field line boundary (Dewey et al., 2017; Lavorenti et al., 2022; Lindsay et al., 2016), and are therefore not connected to the innermost closed field lines of the Mercury dipole field. Thus, we may expect that even during intervals with strong DF activity present, the ∼1 Hz wave activity is not completely lost from the Mercury system. Instead, the innermost region of tightly bound closed field lines may remain sufficiently stable to support prolonged wave activity even during active mid-tail reconfiguration. The systematic confinement of wave activity within 1.3 R_M across the full statistical data set (Figure 3) is consistent with this interpretation, and inconsistent with a simple temporal recovery interpretation, which would instead predict waves at similar radial distances as quiet intervals, just at reduced occurrence rates. Nevertheless, the small residual wave activity observed at larger radial distances during orbits with observed DFs (Figure 3a3) may reflect brief recovery intervals between successive dipolarization events, during which transient stable conditions allow limited wave growth before the next reconfiguration of the magnetic field. Additionally, some contribution from imperfect DF classification cannot be excluded. The automated detection algorithm of Dewey et al. (2020) has a reported detection rate of 73.7% with a false positive rate of 5.0%, meaning that a fraction of orbits may be misclassified between the two groups in Figure 3. Notably, both misclassifications would reduce the contrast between the two groups, suggesting that the statistical trends reported here likely represent a conservative estimate of the true dependence of wave activity on magnetotail reconfiguration. The wave activity for orbits with ≥1 DFs may reflect a combination of confined wave activity on the innermost closed field lines and brief recovery intervals between successive reconfigurations in the highly dynamic magnetosphere of Mercury. This is consistent with the shorter average ridge durations observed during dipolarization orbits, which may also reflect both the smaller spatial region and the rapid temporal recovery time scales (Figure 4). The 1.3 R_M boundary of the wave activity during active conditions corresponds to observed flow breaking distances at Mercury, suggesting that the dipolar field pressure in this region shields inner closed field lines from magnetotail reconfigurations (Cushen et al., 2025; Dewey et al., 2018; Poh et al., 2018; W. J. Sun et al., 2020). This boundary also coincides approximately with the proton plasma beta = 1 contour (Figures 3a1 and 3a2, from Dewey et al., 2020), marking the transition from the magnetically dominated inner region ($\beta < 1$), where stable closed field configurations capable of sustaining particle trapping and ∼1 Hz wave growth are maintained, to the plasma-dominated outer region where magnetotail reconfigurations dominate. The coincidence of the wave occurrence boundary with both the flow breaking distance and the $\beta = 1$ contour therefore provides mutually consistent and independent support for the conclusion that ∼1 Hz wave activity at Mercury is sustained within the innermost magnetically dominated closed field line region, where conditions of sufficient stability for wave growth are most likely to be met.

Mercury's magnetosphere exhibits significant variability in its level of substorm-like activity, which has consequences for the large-scale plasma configuration (Slavin et al., 2018; Zhong et al., 2020). During periods of reduced activity, drift physics dominates, producing nightside asymmetries in proton fluxes, trapped ion populations, and magnetic field structures (Korth et al., 2014; W. J. Sun et al., 2017; Williamson et al., 2026; Zhao et al., 2022). As demonstrated here, these intervals also favor the strong presence of ∼1 Hz wave activity on closed field lines. Conversely, during intervals of frequent DF activity, particularly under strong IMF forcing (Zhong et al., 2023), particle acceleration, heating, and magnetic field reconfigurations reduce the observed plasma asymmetries (Delcourt et al., 2024; Dewey et al., 2018; Poh et al., 2018; W. J. Sun et al., 2017), and suppress the ∼1 Hz wave activity. The ∼1 Hz waves can therefore serve as a new diagnostic of the magnetospheric activity level at Mercury when observed, complementing existing indicators such as plasma asymmetries and DF occurrence rates.

5. Conclusions

In this study, we investigated the connection between the presence of the ∼1 Hz waves on Mercury's closed field lines and the observed dipolarization fronts in the plasma sheet. The results show strong evidence for the mutual

21699402, 2026, 9, Downloaded from https://agupubs.onlinelibrary.wiley.com/doi/10.1029/2026JA035864 by Uppsala University Library, Wiley Online Library on [09/10/2026]. See the Terms and Conditions (https://onlinelibrary.wiley.com/terms-and-conditions) on Wiley Online Library for rules of use; OA articles are governed by the applicable Creative Commons License

exclusivity of the two phenomena, where the ∼1 Hz waves are absent during the orbits containing dipolarization intervals. The ∼1 Hz waves extend to larger downtail distances during quiet intervals and can be maintained for up to 30 min along the spacecraft trajectory, while being confined to the innermost closed field line region during much shorter intervals during active periods, indicating the importance of magnetic stability in both their generation and maintenance.

The lack of ∼1 Hz wave activity during active magnetic reconfiguration time intervals can be understood in terms of the plasma time scales. The dipolarization events typically occur on the same time scale as the bounce period of protons on newly closed field lines, on the order of 10 s. This, together with the heating and acceleration of protons during dipolarization events, means that the ions cannot develop strong ion anisotropies. While this study does not directly identify the physical generation mechanism of the ∼1 Hz waves, or determine their wave mode, the observed waves require some form of free energy to grow. These results are consistent with ion loss cone anisotropies providing this free energy, which require stable field line conditions to develop and cannot be maintained during rapid magnetotail reconfiguration. Nevertheless, the waves are observed during only 10%–20% of quiet intervals, suggesting that magnetic stability is a necessary but not sufficient condition for wave growth, with additional requirements such as specific particle distribution thresholds remaining to be quantified.

The results therefore show that the strong presence of ∼1 Hz waves is indicative of tail stability at Mercury, and can be used as a diagnostic of the magnetospheric activity level. Their presence marks long-lived, stable closed flux tubes with sustained particle trapping, while their absence or reduced occurrence is statistically associated with intervals of ongoing magnetic reconfiguration. However, as ∼1 Hz waves are observed only ∼10%–20% of the time, even under favorable conditions, the absence of waves on any given orbit cannot be confidently interpreted as an indicator of a disturbed magnetosphere or active reconnection. Their presence is therefore a more reliable single-event diagnostic than their absence. Nevertheless, this establishes a connection between field-line history, magnetospheric activity, and wave occurrence in Mercury's magnetotail.

The future BepiColombo mission's improved particle instrumentation will be uniquely suited to measuring proton pitch-angle distributions on stable closed field lines and during dipolarization intervals, providing a definitive test of whether loss-cone anisotropies are present under the stable conditions identified here. The two-point measurements will allow further constraints on the stability and generation of the ∼1 Hz waves, and the new combined electric and magnetic field measurements can be used to directly constrain the wave mode responsible for the ∼1 Hz oscillations. Such observations will directly build on the constraints established here, advancing our understanding of wave-particle interactions in Mercury's uniquely dynamic magnetosphere.

Conflict of Interest

The authors declare no conflicts of interest relevant to this study.

Availability Statement

The high-resolution magnetometer data from the fluxgate magnetometer onboard MESSENGER (Anderson et al., 2007) used in this study are publicly available for download at the NASA Planetary Data System (Korth, 2021; https://doi.org/10.17189/1522385). The Mercury Disturbance Index (MDI) was derived from the MESSENGER MAG KT17 model residuals data set (Korth, 2022; https://doi.org/10.17189/ZYSM-MN42). FIPS proton energy spectra (Andrews et al., 2007) are publicly available at the NASA Planetary Data System (Raines, 2016; https://doi.org/10.17189/1523000). The bow shock and magnetopause crossing database is taken from W. Sun (2023), available at Zenodo (https://doi.org/10.5281/ZENODO.8298647).

Acknowledgments

The authors acknowledge all members of the MESSENGER mission, in particular the magnetometer team, for their contributions to the success of the mission. M.P. gratefully acknowledges support from the Swedish National Space Agency (SNSA) (Dnr 2023-00183). R.D. was supported by NASA Planetary Science Division Grants 80NSSC24K0059, 80NSSC25K0038, 80NSSC24K1777. E.Y. research is funded by SNSA Grant 2024-00209.

References

Alberti, T., Consolini, G., Carbone, V., Yordanova, E., Marcucci, M. F., & De Michelis, P. (2019). Multifractal and chaotic properties of solar wind at MHD and kinetic domains: An empirical mode decomposition approach. *Entropy*, *21*(3), 320. https://doi.org/10.3390/e21030320

Alexeev, I. I., Belenkaya, E. S., Slavin, J. A., Korth, H., Anderson, B. J., Baker, D. N., et al. (2010). Mercury's magnetospheric magnetic field after the first two MESSENGER flybys. *Icarus*, *209*(1), 23–39. https://doi.org/10.1016/j.icarus.2010.01.024

Anderson, B. J., Acuña, M. H., Korth, H., Slavin, J. A., Uno, H., Johnson, C. L., et al. (2010). The magnetic field of Mercury. *Space Science Reviews*, *152*(1–4), 307–339. https://doi.org/10.1007/s11214-009-9544-3

Anderson, B. J., Acuna, M. H., Lohr, D. A., Scheifele, J., Raval, A., Korth, H., & Slavin, J. A. (2007). The magnetometer instrument on MESSENGER. In D. L. Domingue & C. T. Russell (Eds.), *The messenger mission to Mercury* (pp. 417–450). Springer. https://doi.org/10.1007/978-0-387-77214-1_12

Anderson, B. J., Johnson, C. L., & Korth, H. (2013). A magnetic disturbance index for Mercury's magnetic field derived from MESSENGER magnetometer data. *Geochemistry, Geophysics, Geosystems*, *14*(9), 3875–3886. https://doi.org/10.1002/ggge.20242

Anderson, B. J., Johnson, C. L., Korth, H., Purucker, M. E., Winslow, R. M., Slavin, J. A., et al. (2011). The global magnetic field of Mercury from MESSENGER orbital observations. *Science*, *333*(6051), 1859–1862. https://doi.org/10.1126/science.1211001

Anderson, B. J., Johnson, C. L., Korth, H., Winslow, R. M., Borovsky, J. E., Purucker, M. E., et al. (2012). Low-degree structure in Mercury's planetary magnetic field. *Journal of Geophysical Research*, *117*(E12). https://doi.org/10.1029/2012JE004159

Andrews, G. B., Zurbuchen, T. H., Mauk, B. H., Malcom, H., Fisk, L. A., Gloeckler, G., et al. (2007). The energetic particle and plasma spectrometer instrument on the MESSENGER spacecraft. *Space Science Reviews*, *131*(1–4), 523–556. https://doi.org/10.1007/s11214-007-9272-5

Boardsen, S. A., Anderson, B. J., Acuña, M. H., Slavin, J. A., Korth, H., & Solomon, S. C. (2009). Narrow-band ultra-low-frequency wave observations by MESSENGER during its January 2008 flyby through Mercury's magnetosphere. *Geophysical Research Letters*, *36*(1). https://doi.org/10.1029/2008GL036034

Boardsen, S. A., Kim, E.-H., Raines, J. M., Slavin, J. A., Gershman, D. J., Anderson, B. J., et al. (2015). Interpreting 1 Hz magnetic compressional waves in Mercury's inner magnetosphere in terms of propagating ion-Bernstein waves. *Journal of Geophysical Research: Space Physics*, *120*(6), 4213–4228. https://doi.org/10.1002/2014JA020910

Boardsen, S. A., Slavin, J. A., Anderson, B. J., Korth, H., Schriver, D., & Solomon, S. C. (2012). Survey of coherent ∼1 Hz waves in Mercury's inner magnetosphere from MESSENGER observations. *Journal of Geophysical Research*, *117*(A12). https://doi.org/10.1029/2012JA017822

Carbone, F., Sorriso-Valvo, L., Alberti, T., Lepreti, F., Chen, C. H. K., Němeček, Z., & Šafránková, J. (2018). Arbitrary-order Hilbert spectral analysis and intermittency in solar wind density fluctuations. *The Astrophysical Journal*, *859*(1), 27. https://doi.org/10.3847/1538-4357/aabcc2

Cushen, A. T., Sun, W., Slavin, J., Dewey, R., Jia, X., & Zhao, J. (2025). Dipolarization regions in Mercury's magnetosphere: Observation of flux pileup and formation of a substorm current wedge. *Geophysical Research Letters*, *52*(24), e2025GL117281. https://doi.org/10.1029/2025GL117281

Dagore, A., Prete, G., Capparelli, V., Carbone, V., & Lepreti, F. (2026). Analysing turbulent energy cascade in a coronal mass ejection using empirical mode decomposition. *Astronomy & Astrophysics*, *713*, A46. https://doi.org/10.1051/0004-6361/202557398

Delcourt, D., Hadid, L. Z., & Aizawa, S. (2024). On the response of protons to dynamical reconfigurations of Mercury's magnetosphere. *Geophysical Research Letters*, *51*(21), e2024GL110351. https://doi.org/10.1029/2024GL110351

Dewey, R. M., Raines, J. M., Sun, W., Slavin, J. A., & Poh, G. (2018). MESSENGER observations of fast plasma flows in Mercury's magnetotail. *Geophysical Research Letters*, *45*(19), 10110–10118. https://doi.org/10.1029/2018GL079056

Dewey, R. M., Slavin, J. A., Raines, J. M., Azari, A. R., & Sun, W. (2020). MESSENGER observations of flow braking and flux pileup of dipolarizations in Mercury's magnetotail: Evidence for current wedge formation. *Journal of Geophysical Research: Space Physics*, *125*(9), e2020JA028112. https://doi.org/10.1029/2020JA028112

Dewey, R. M., Slavin, J. A., Raines, J. M., Baker, D. N., & Lawrence, D. J. (2017). Energetic electron acceleration and injection during dipolarization events in Mercury's magnetotail. *Journal of Geophysical Research: Space Physics*, *122*(12), 12170–12188. https://doi.org/10.1002/2017JA024617

Gershman, D. J., Slavin, J. A., Raines, J. M., Zurbuchen, T. H., Anderson, B. J., Korth, H., et al. (2014). Ion kinetic properties in Mercury's pre-midnight plasma sheet. *Geophysical Research Letters*, *41*(16), 5740–5747. https://doi.org/10.1002/2014GL060468

Glass, A. N., Raines, J. M., Jia, X., Sun, W., Imber, S., Dewey, R. M., & Slavin, J. A. (2022). Observations of Mercury's plasma sheet horn: Characterization and contribution to proton precipitation. *Journal of Geophysical Research: Space Physics*, *127*(12), e2022JA030969. https://doi.org/10.1029/2022JA030969

Huang, N. E., Shen, Z., Long, S. R., Wu, M. C., Shih, H. H., Zheng, Q., et al. (1998). The empirical mode decomposition and the Hilbert spectrum for nonlinear and non-stationary time series analysis. *Proceedings of the Royal Society A: Mathematical, Physical and Engineering Sciences*, *454*(1971), 903–995. https://doi.org/10.1098/rspa.1998.0193

Imber, S. M., & Slavin, J. A. (2017). MESSENGER observations of magnetotail loading and unloading: Implications for substorms at Mercury. *Journal of Geophysical Research: Space Physics*, *122*(11), 11402–11412. https://doi.org/10.1002/2017JA024332

Jia, X., Slavin, J. A., Poh, G., DiBraccio, G. A., Toth, G., Chen, Y., et al. (2019). MESSENGER observations and global simulations of highly compressed magnetosphere events at Mercury. *Journal of Geophysical Research: Space Physics*, *124*(1), 229–247. https://doi.org/10.1029/2018JA026166

Kim, E.-H., Boardsen, S. A., Johnson, J. R., & Slavin, J. A. (2016). ULF waves at Mercury. In *Low-frequency waves in space plasmas* (pp. 323–341). American Geophysical Union (AGU). https://doi.org/10.1002/9781119055006.ch19

Kim, E.-H., Johnson, J. R., Lee, D.-H., & Pyo, Y. S. (2013). Field-line resonance structures in Mercury's multi-ion magnetosphere. *Earth Planets and Space*, *65*(5), 447–451. https://doi.org/10.5047/eps.2012.08.004

Kim, E.-H., Johnson, J. R., & Lee, K.-D. (2011). ULF wave absorption at Mercury. *Geophysical Research Letters*, *38*(16). https://doi.org/10.1029/2011GL048621

Kim, E.-H., Johnson, J. R., Valeo, E., & Phillips, C. K. (2015). Global modeling of ULF waves at Mercury. *Geophysical Research Letters*, *42*(13), 5147–5154. https://doi.org/10.1002/2015GL064531

Korth, H. (2021). MESSENGER MAG calibrated MSO coordinates science data collection [Dataset]. *NASA Planetary Data System*. https://doi.org/10.17189/1522385

Korth, H. (2022). MESSENGER magnetometer KT17 model Mercury solar orbital (MSO) residual data [Dataset]. *NASA Planetary Data System*. https://doi.org/10.17189/zysm-mn42

Korth, H., Anderson, B. J., Gershman, D. J., Raines, J. M., Slavin, J. A., Zurbuchen, T. H., et al. (2014). Plasma distribution in Mercury's magnetosphere derived from MESSENGER magnetometer and fast imaging plasma spectrometer observations. *Journal of Geophysical Research: Space Physics*, *119*(4), 2917–2932. https://doi.org/10.1002/2013JA019567

Korth, H., Anderson, B. J., Raines, J. M., Slavin, J. A., Zurbuchen, T. H., Johnson, C. L., et al. (2011). Plasma pressure in Mercury's equatorial magnetosphere derived from MESSENGER magnetometer observations. *Geophysical Research Letters*, *38*(22). https://doi.org/10.1029/2011GL049451

Korth, H., Johnson, C. L., Philpott, L., Tsyganenko, N. A., & Anderson, B. J. (2017). A dynamic model of Mercury's magnetospheric magnetic field. *Geophysical Research Letters*, *44*(20), 10147–10154. https://doi.org/10.1002/2017GL074699

Lavorenti, F., Henri, P., Califano, F., Deca, J., Aizawa, S., André, N., & Benkhoff, J. (2022). Electron dynamics in small magnetospheres–Insights from global, fully kinetic plasma simulations of the planet Mercury. *Astronomy & Astrophysics*, *664*, A133. https://doi.org/10.1051/0004-6361/202243911

Li, X., Dong, C., Wang, L., Aizawa, S., Hadid, L. Z., Zhang, C., et al. (2026). Spectral properties and energy injection in Mercury's magnetotail current sheet. *Geophysical Research Letters*, *53*(4), e2025GL120144. https://doi.org/10.1029/2025GL120144

21699402, 2026, 9, Downloaded from https://agupubs.onlinelibrary.wiley.com/doi/10.1029/2026JA035864 by Uppsala University Library, Wiley Online Library on [09/10/2026]. See the Terms and Conditions (https://onlinelibrary.wiley.com/terms-and-conditions) on Wiley Online Library for rules of use; OA articles are governed by the applicable Creative Commons License

Lindsay, S. T., James, M. K., Bunce, E. J., Imber, S. M., Korth, H., Martindale, A., & Yeoman, T. K. (2016). MESSENGER X-ray observations of magnetosphere–surface interaction on the nightside of Mercury. *Planetary and Space Science*, *125*, 72–79. https://doi.org/10.1016/j.pss.2016.03.005

Othmer, C., Glassmeier, K.-H., & Cramm, R. (1999). Concerning field line resonances in Mercury's magnetosphere. *Journal of Geophysical Research*, *104*, 10369–10378. https://doi.org/10.1029/1999JA900009

Persson, M., Dimmock, A. P., Wahlund, J.-E., Morooka, M., Yordanova, E., Eriksson, A. I., et al. (2026). Occurrence and controls of ∼1 Hz waves in Mercury's magnetosphere: Insights from MESSENGER observations. *Earth Planets and Space*, *78*, 180. https://doi.org/10.1186/s40623-026-02516-6

Poh, G., Slavin, J. A., Jia, X., Raines, J. M., Imber, S. M., Sun, W.-J., et al. (2017). Mercury's cross-tail current sheet: Structure, X-line location and stress balance. *Geophysical Research Letters*, *44*(2), 678–686. https://doi.org/10.1002/2016GL071612

Poh, G., Slavin, J. A., Jia, X., Sun, W.-J., Raines, J. M., Imber, S. M., et al. (2018). Transport of mass and energy in Mercury's plasma sheet. *Geophysical Research Letters*, *45*(22), 12163–12170. https://doi.org/10.1029/2018GL080601

Raines, J. M. (2016). MESSENGER EPPS FIPS derived bundle [Dataset]. *NASA Planetary Data System*. https://doi.org/10.17189/1523000

Richard, L., Khotyaintsev, Y. V., Graham, D. B., & Russell, C. T. (2022). Are dipolarization fronts a typical feature of magnetotail plasma jets fronts? *Geophysical Research Letters*, *49*(22), e2022GL101693. https://doi.org/10.1029/2022GL101693

Richard, L., Sorriso-Valvo, L., Yordanova, E., Graham, D. B., & Khotyaintsev, Y. V. (2024). Turbulence in magnetic reconnection jets from injection to sub-ion scales. *Physical Review Letters*, *132*(10), 105201. https://doi.org/10.1103/PhysRevLett.132.105201

Russell, C. T. (1989). ULF waves in the Mercury magnetosphere. *Geophysical Research Letters*, *16*(11), 1253–1256. https://doi.org/10.1029/GL016i011p01253

Slavin, J. A., Acuña, M. H., Anderson, B. J., Baker, D. N., Benna, M., Boardsen, S. A., et al. (2009). MESSENGER observations of magnetic reconnection in Mercury's magnetosphere. *Science*, *324*(5927), 606–610. https://doi.org/10.1126/science.1172011

Slavin, J. A., Anderson, B. J., Baker, D. N., Benna, M., Boardsen, S. A., Gloeckler, G., et al. (2010). MESSENGER observations of extreme loading and unloading of Mercury's magnetic tail. *Science*, *329*(5992), 665–668. https://doi.org/10.1126/science.1188067

Slavin, J. A., Baker, D. N., Gershman, D. J., Ho, G. C., Imber, S. M., Krimigis, S. M., & Sundberg, T. (2018). Mercury's dynamic magnetosphere. In B. J. Anderson, L. R. Nittler, & S. C. Solomon (Eds.), *Mercury: The view after MESSENGER, Cambridge planetary science* (pp. 461–496). Cambridge University Press. https://doi.org/10.1017/9781316650684.018

Slavin, J. A., Imber, S. M., & Raines, J. M. (2021). A Dungey cycle in the life of Mercury's magnetosphere. In *Magnetospheres in the solar system* (pp. 535–556). American Geophysical Union (AGU). https://doi.org/10.1002/9781119815624.ch34

Slavin, J. A., Middleton, H. R., Raines, J. M., Jia, X., Zhong, J., Sun, W.-J., et al. (2019). MESSENGER observations of disappearing dayside magnetosphere events at Mercury. *Journal of Geophysical Research: Space Physics*, *124*(8), 6613–6635. https://doi.org/10.1029/2019JA026892

Solomon, S. C., McNutt, R. L., Gold, R. E., & Domingue, D. L. (2007). MESSENGER mission overview. *Space Science Reviews*, *131*(1–4), 3–39. https://doi.org/10.1007/s11214-007-9247-6

Sun, W. (2023). Lists of magnetopause and bow shock crossings of mercury by MESSENGER spacecraft [Dataset]. *Zenodo*. https://doi.org/10.5281/ZENODO.8298647

Sun, W., Dewey, R. M., Aizawa, S., Huang, J., Slavin, J. A., Fu, S., et al. (2022). Review of Mercury's dynamic magnetosphere: Post-MESSENGER era and comparative magnetospheres. *Science China Earth Sciences*, *65*(1), 25–74. https://doi.org/10.1007/s11430-021-9828-0

Sun, W. J., Raines, J. M., Fu, S. Y., Slavin, J. A., Wei, Y., Poh, G. K., et al. (2017). MESSENGER observations of the energization and heating of protons in the near-Mercury magnetotail. *Geophysical Research Letters*, *44*(16), 8149–8158. https://doi.org/10.1002/2017GL074276

Sun, W. J., Slavin, J. A., Dewey, R. M., Chen, Y., DiBraccio, G. A., Raines, J. M., et al. (2020). MESSENGER observations of Mercury's nightside magnetosphere under extreme solar wind conditions: Reconnection-generated structures and steady convection. *Journal of Geophysical Research: Space Physics*, *125*(3), e2019JA027490. https://doi.org/10.1029/2019JA027490

Sun, W. J., Slavin, J. A., Dewey, R. M., Raines, J. M., Fu, S. Y., Wei, Y., et al. (2018). A comparative study of the proton properties of magnetospheric substorms at Earth and Mercury in the near magnetotail. *Geophysical Research Letters*, *45*(16), 7933–7941. https://doi.org/10.1029/2018GL079181

Sundberg, T., Slavin, J. A., Boardsen, S. A., Anderson, B. J., Korth, H., Ho, G. C., et al. (2012). MESSENGER observations of dipolarization events in Mercury's magnetotail. *Journal of Geophysical Research*, *117*(A12). https://doi.org/10.1029/2012JA017756

Torrence, C., & Compo, G. P. (1998). A practical guide to wavelet analysis. *Bulletin of the American Meteorological Society*, *79*(1), 61–78. https://doi.org/10.1175/1520-0477(1998)079<0061:apgtwa>2.0.co;2

Williamson, H. N., Barabash, S., Nilsson, H., Wieser, M., Raines, J. M., Milillo, A., et al. (2026). BepiColombo at Mercury: Three flybys, three magnetospheres. *Geophysical Research Letters*, *53*(2), e2025GL119589. https://doi.org/10.1029/2025GL119589

Winslow, R. M., Anderson, B. J., Johnson, C. L., Slavin, J. A., Korth, H., Purucker, M. E., et al. (2013). Mercury's magnetopause and bow shock from MESSENGER magnetometer observations. *Journal of Geophysical Research: Space Physics*, *118*(5), 2213–2227. https://doi.org/10.1002/jgra.50237

Winslow, R. M., Lugaz, N., Philpott, L., Farrugia, C. J., Johnson, C. L., Anderson, B. J., et al. (2020). Observations of extreme ICME ram pressure compressing Mercury's dayside magnetosphere to the surface. *The Astrophysical Journal*, *889*(2), 184. https://doi.org/10.3847/1538-4357/ab6170

Zhao, J.-T., Zong, Q.-G., Slavin, J. A., Sun, W.-J., Zhou, X.-Z., Yue, C., et al. (2020). Proton properties in Mercury's magnetotail: A statistical study. *Geophysical Research Letters*, *47*(19), e2020GL088075. https://doi.org/10.1029/2020GL088075

Zhao, J.-T., Zong, Q.-G., Yue, C., Sun, W.-J., Zhang, H., Zhou, X.-Z., et al. (2022). Observational evidence of ring current in the magnetosphere of Mercury. *Nature Communications*, *13*(1), 924. https://doi.org/10.1038/s41467-022-28521-3

Zhong, J., Lee, L.-C., Slavin, J. A., Zhang, H., & Wei, Y. (2023). MESSENGER observations of reconnection in Mercury's magnetotail under strong IMF forcing. *Journal of Geophysical Research: Space Physics*, *128*(2), e2022JA031134. https://doi.org/10.1029/2022JA031134

Zhong, J., Lee, L. C., Wang, X. G., Pu, Z. Y., He, J. S., Wei, Y., & Wan, W. X. (2020). Multiple X-line reconnection observed in Mercury's magnetotail driven by an interplanetary coronal mass ejection. *The Astrophysical Journal Letters*, *893*(1), L11. https://doi.org/10.3847/2041-8213/ab8380

Zhong, J., Wan, W. X., Slavin, J. A., Wei, Y., Lin, R. L., Chai, L. H., et al. (2015). Mercury's three-dimensional asymmetric magnetopause. *Journal of Geophysical Research: Space Physics*, *120*(9), 7658–7671. https://doi.org/10.1002/2015JA021425

Zhong, J., Wan, W. X., Wei, Y., Slavin, J. A., Raines, J. M., Rong, Z. J., et al. (2015). Compressibility of Mercury's dayside magnetosphere. *Geophysical Research Letters*, *42*(23), 10135–10139. https://doi.org/10.1002/2015GL067063

Zhong, J., Wei, Y., Pu, Z. Y., Wang, X. G., Wan, W. X., Slavin, J. A., et al. (2018). MESSENGER observations of rapid and impulsive magnetic reconnection in Mercury's magnetotail. *The Astrophysical Journal Letters*, *860*(2), L20. https://doi.org/10.3847/2041-8213/aaca92

Zhong, J., Zong, Q. G., Wei, Y., Slavin, J. A., Cao, X., Pu, Z. Y., et al. (2019). MESSENGER observations of giant plasmoids in Mercury's magnetotail. *The Astrophysical Journal Letters*, *886*(2), L32. https://doi.org/10.3847/2041-8213/ab5650

21699402, 2026, 9, Downloaded from https://agupubs.onlinelibrary.wiley.com/doi/10.1029/2026JA035864 by Uppsala University Library, Wiley Online Library on [09/10/2026]. See the Terms and Conditions (https://onlinelibrary.wiley.com/terms-and-conditions) on Wiley Online Library for rules of use; OA articles are governed by the applicable Creative Commons License